remote sensing

MDPI

Article

Sea Ice Freeboard in the Ross Sea from Airborne Altimetry IcePod 2016–2017 and a Comparison with IceBridge 2013 and ICESat 2003–2008

Liuxi Tian [1,2], Hongjie Xie [1,2,*], Stephen F. Ackley [1,2], Kirsty J. Tinto [3], Robin E. Bell [3], Christopher J. Zappa [3], Yongli Gao [1,2] and Alberto M. Mestas-Nuñez [1,2]

1 Department of Geological Sciences, University of Texas at San Antonio, San Antonio, TX 78249, USA; liuxi.tian@my.utsa.edu (L.T.); stephen.ackley@utsa.edu (S.F.A.); yongli.gao@utsa.edu (Y.G.); alberto.mestas@utsa.edu (A.M.M.-N.)

2 NASA Center for Advanced Measurements in Extreme Environments, University of Texas at San Antonio, San Antonio, TX 78249, USA

3 Lamont-Doherty Earth Observatory, Columbia University, New York, NY 10964, USA; tinto@ldeo.columbia.edu (K.J.T.); robinb@ldeo.columbia.edu (R.E.B.); zappa@ldeo.columbia.edu (C.J.Z.)

* Correspondence: hongjie.xie@utsa.edu; Tel.: +1-210-4585445

Received: 27 May 2020; Accepted: 9 July 2020; Published: 11 July 2020

Abstract: As part of the Polynyas and Ice Production in the Ross Sea (PIPERS) project, the IcePod system onboard the LC-130 aircraft based at McMurdo Station was flown over the Ross Sea, Antarctica in November 2016 and 2017, with the purpose of repeating the same lines that NASA's Operation IceBridge (OIB) aircraft flew over in 2013. We resampled the lidar data into 70 m pixels (similar to the footprint size of OIB L2 and ICESat data) and took the mean of the lowest 2% elevation values of 25 km (50 km) length along a flight track as the local sea level of the central 25 km (50 km). Most of the IcePod data were over the same flight lines taken by OIB in 2013, so the total freeboard changes from 2013 to 2016 and 2017 were examined. Combining with the ICESat (2003–2008), we obtained a better picture of total freeboard and its interannual variability in the Ross Sea. The pattern of the sea ice distribution supports that new ice produced in coastal polynyas was transported northward by katabatic winds off the ice shelf. Compared to ICESat years, sea ice near the coast was thicker, while sea ice offshore was thinner in the more recent OIB/IcePod years. The results also showed that, in general, sea ice was thicker in 2017 compared to 2013 or 2016—0.02–0.55 m thicker in total freeboard.

Keywords: Antarctic; polynya; ice production; local sea level; laser altimetry

1. Introduction

Sea ice in the polar regions plays a critical part in climate change because of its impact and feedback on the transfer of energy across the ocean–atmosphere interface [1,2]. The Ross Sea is of considerable interest because of its positive trend in sea ice extent. In the context of global warming, the Ross Sea's increased sea ice extent and duration during the last few decades are in contrast with the decreases observed in the Arctic from passive microwave satellite data [3,4]; though in the last four years, the trend has changed with a sharp decline in the extent that the first occurred in the late 2016 [5–7]. But the changes in sea ice thickness, volume, and production in this region are still unclear. Without knowing the changes in the sea ice thickness over the Ross Sea, it is hard to evaluate how sea ice cover is responding to a changing climate in this region. There are three polynyas—Ross Ice Shelf polynya (RISP), Terra Nova Bay polynya (TNB), and McMurdo Sound polynya (MCM)—in the Ross Sea. These polynyas are the high rates of sea ice production areas, as older sea ice is continually blown offshore and replaced by newly formed ice [8]. This causes dense water formation by brine rejection

and thereby contributes to the formation of Antarctic bottom water (AABW). Knowing the interannual variability of the sea ice thickness in the Ross Sea is crucial to the estimation of sea ice production and better knowledge of the energy exchange between ocean and atmosphere as well as improvement of model prediction [9].

A variety of tools and techniques have been used to measure sea ice thickness including direct measurements by drilling a hole through the ice [10], using electromagnetic induction techniques [11], and installing ice mass balance buoys. More recently, airborne and satellite-borne laser altimetry data have been wildly used to extract ice or total freeboard and then derive sea ice thickness [12–15]. Total freeboard, the sum of the snow depth and ice freeboards, is the height of the air-snow interface above the local sea surface [16–18]. In this study, we aimed to use three datasets with laser altimetry, IcePod 2016–2017, NASA's Operation IceBridge (OIB) 2013, and ICESat 2003–2008 to get the total freeboard data by using the same method and then investigate the patterns of interannual variations of total freeboard (corresponding to sea ice thickness) in the Ross Sea.

The OIB mission flew over the Ross Sea, Antarctica (November 2013) and collected important sea ice data with the Airborne Topographic Mapper (ATM) and Digital Mapping System (DMS) instrumentation for the first time [19]. The ATM lidar data measure the elevation of the sea ice and the DMS can be used to identify open water. As part of the Polynyas and Ice Production in the Ross Sea (PIPERS) project [20], the IcePod system with similar instrumentation, including a scanning laser for ice surface measurements, visible and thermal infrared imaging cameras for ice surface identification, two different radar systems, magnetometer, and gravimeter, onboard the NSF LC-130 aircraft based at McMurdo Station was flown over the Ross Sea, Antarctica in November 2016 and 2017. The purpose of IcePod flights was to repeat the approximate same lines that NASA's OIB aircraft flew over in November 2013, particularly the line along the Fluxgate which separates the continental shelf from the deep ocean (Shelf-Slope break). The IcePod is an externally mounted modular sensor and data acquisition system that can be attached and detached relatively easily from a LC-130 airplane [21].

In a recent study [22], the OIB 2013 data were used to analyze the distribution of sea ice over the Ross Sea. The goal of this study was to investigate the patterns of interannual variations of total freeboard (sea ice thickness) in the Ross Sea by comparing the IcePod 2016–2017 data with both the OIB 2013 and the ICESat 2003–2008 data. The body of this paper is organized as follows: a description of the datasets and of the study area are given in Section 2; the methods leading to the calculation of total freeboard are presented in Section 3; and the comparison results are presented in Section 4. The paper ends with a discussion of the results in Section 5 and final conclusions in Section 6.

2. Study Area and Datasets

The four flight tracks in Ross Sea lie downstream of the Antarctic coastal polynyas, the Ross Ice Shelf Polynya (RSP), the Terra Nova Bay polynya (TNB), and McMurdo Sound polynya (MCM) (Figure 1). Coastal polynyas are areas where much of the Ross Sea ice production takes place and the released salt flux leads to AABW formation [8] in the region. The Ross Sea fluxgate, separating the continental shelf from the deep ocean, roughly lies over the 1000 m isobath [23] and is used to calculate ice production and ice export from over the Ross Sea continental shelf to over the deep ocean. Overall, the track 1 is parallel to major outlet glaciers extends from Ross Island to north of Terra Nova Bay. The ice along the track 1 tends to be rougher with thinner ice passing through Terra Nova Bay. The track 2, mostly in north Victoria land, is similarly coast parallel, crossing outlet glaciers that extend to have relatively thicker but inhomogeneous ice thickness. The track 3 is an indication of ice conditions in the center of the Ross Sea and where the sea ice is generally thinner. The track 4 is along the continental shelf fluxgate with mostly thin ice, having thicker ice close to the coast of Cape Adare.

Three datasets used in this study are IcePod (2016–2017), OIB ATM L2 (2013), and ICESat (2003–2008) (Table 1). The IcePod system is operated by the Lamont–Doherty Earth Observatory (LDEO) at Columbia University in New York. The lidar instrument on board the IcePod is a Riegl VQ-580 airborne laser scanner which is specifically designed for use over snow and ice. The laser

transmits pulses at a near infrared 1064 nm wavelength over a 60 degree field of view [24]. At the survey elevation of 3000 ft (~914 m) above ground level and survey ground speed of 170 knots (~87 m/s), the spot size on the ground is 20 cm and the point density is 1.2 pixels/m^2.

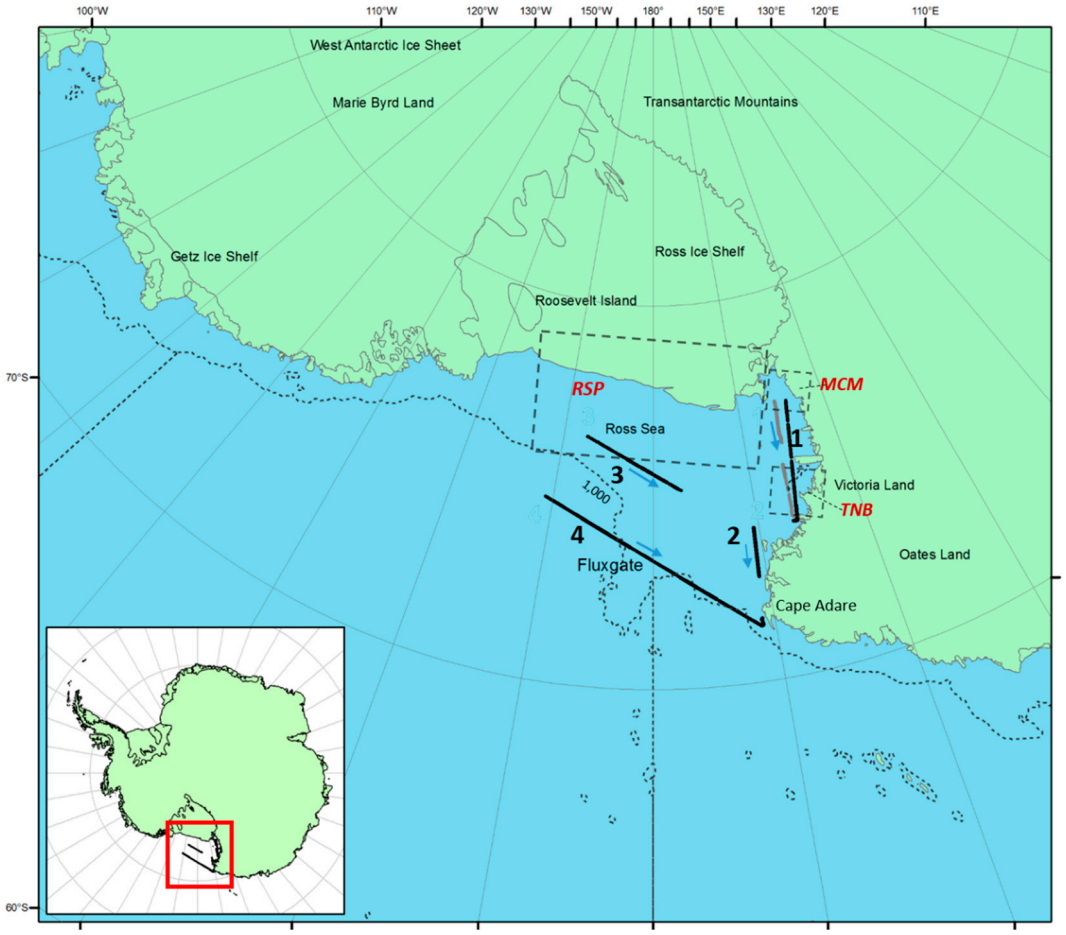

Figure 1. Map of the Ross Sea showing the IcePod flight tracks 1–4 used in this study. Tracks 1, 3, and 4 repeat the Operation IceBridge 2013 lines. For track 1, the IcePod track (black) did not exactly locate over the OIB track (grey). Track 4 is the line identified as the Ross Sea Fluxgate roughly over the 1000 m bathymetry contour (dotted line). The arrows show the direction of each track that is used for distance calculation. Dashed rectangles indicate locations of the Ross Ice Shelf polynya (RSP), Terra Nova Bay polynya (TNB), and McMurdo Sound polynya (MCM).

Table 1. The datasets with acquisition time and corresponding tracks used in this study. (ICESat track here is a pseudo track, i.e., ICESat data within 30 km each side of the central IcePod track; refer to Figure 12 of Reference [22]).

Dataset	Acquisition Time	Tracks
ICESat	2003, 09/25–11/18	1,3,4
ICESat	2004, 10/03–11/08	1,2,3,4
ICESat	2005, 10/21–11/23	1,2,3,4
ICESat	2006, 10/25–11/27	1,2,3,4
ICESat	2007, 10/02–11/04	1,2,3,4
ICESat	2008, 10/04–10/18	2,3,4
OIB	2013, 11/20 and 11/27	1,3,4
IcePod	2016, 11/27 and 11/28	1,2,
IcePod	2017, 11/21 and 11/22	1,2,3,4

The OIB laser scanner (ATM) is a conically scanning laser altimeter of using 532 nm wavelength, with a pulse repetition frequency of 5 kHz and an off-nadir scan angle of ~15° (T2 scanner) or 23° (T3 scanner) [25]. The ATM L2 data are the resampled data at the distance interval averaging 0.5 s (approximately 60 m) worth of data along the flight track and a fixed 80 m across-track nadir platelet as well as three or five additional platelets that together span the entire swath of the ATM scan [19].

The ICESat was launched by NASA in 2003 with a Geoscience Laser Altimeter System (GLAS) for measuring surface elevations by using the 1064 nm channel [26]. It sampled the Earth's surface from an orbit with an inclination of 94° with footprints of ~70 m in diameter spaced at ~170 m intervals [27]. In this study, we used the ICESat freeboard product (2003–2008) which was derived using a local sea-level reference obtained by the lowest (2%) elevation values within a 50 km section [28]. In order for ICESat data to have sufficient footprints to do statistics and for comparison, the full spring seasons of ICESat data (Table 1) were used to extract the corresponding ICESat data along each IcePod track (within a distance of 30 km at each side of an IcePod track).

3. Methods

3.1. Preprocessing of OIB and IcePod Dataset

To make the results comparable among the three datasets, we resampled the IcePod lidar data into 70 m pixels (by averaging 70 m width by 70 m along track window), since they were comparable to the footprint size of OIB ATM L2 (80 m width by ~60 m along track) and ICESat data resolution (~70 m). Laser altimetry detects the sea surface height (SSH). Both OIB and IcePod lidar data were providing SSH in meters above the WGS1984 ellipsoid. The SSH was influenced by geoid, tidal forces, atmospheric pressure, and ocean dynamic topography [29]. The DTU15 Mean Sea Surface (MSS) released from DTU (Technical University of Denmark) is a global, high-resolution MSS with a resolution of 1 min by 1 min [30]. The DTU15 MSS comprises geoid undulation and ocean mean dynamic topography which are the largest variations of SSH. The preprocessing of OIB and IcePod dataset were to remove those MSS influences from SSH. We obtained Sea Surface Height Anomalies (SSHAs) by using SSHs minus the DTU15 MSS. These SSHAs were used to calculate total freeboard detailed below.

3.2. Obtain Total Freeboard

In this study, as we used the ICESat total freeboard products (2003–2008), only OIB and IcePod were needed to calculate total freeboard. To obtain freeboard, the local sea level reference must be determined first. There are several methods to obtain local sea level reference. The first is to use a percentage of the lowest elevation points along a flight track range and then calculates the average height of these points as the local sea level [31]. We call this "the lowest elevation method" in this study. The other methods include local sea identification from apparent reflectivity, waveform characteristics, or optical images [22]. As ICESat freeboard products (2003–2008) were derived by using a local sea level reference obtained by the lowest (2%) elevation values within a 50 km section [28], we used the lowest elevation method for OIB and IcePod, so the results were comparable among all three datasets. We assumed 2% of SSHA values as the lowest elevation points along the distance of 25 km and 50 km flight tracks as sea surface shots for both IcePod and OIB. Then the total freeboard of each pixel (OIB ATM L2 or resampled IcePod) could be calculated by differencing this elevation from the SSHA values at the center pixel along the 25 km or 50 km track length. There are different methods to calculate ice thickness from total freeboard and each method would bring different uncertainties. For the purpose of this paper, we only compared the total ice freeboard which is the real data that should be compared.

4. Results

Figure 2 shows the spatial distribution of total freeboard values along the tracks (1, 2, 3, 4) of IcePod (2016–2017) and OIB (2013). Track 1 is a south–north (S–N) track parallel to the coast and the whole track length was approximately 340 km. The sea ice had the lowest freeboard at the southern

end. while it had the highest at the northern end of this track (also seen in Figure 3). Track 2 (~140 km) was the shortest track and sea ice along this track was thicker than the other tracks in general. Sea ice along track 3 (~310 km) was the thinnest and mostly level ice, i.e., small variation of freeboard (also seen in Figure 4). The derived total freeboard along the whole pf track 3 were less than 0.3 m (also seen in Figure 4). Track 4 (the fluxgate) was the longest track (~730 km) with thicker ice in the northwest, where it was close to the coast.

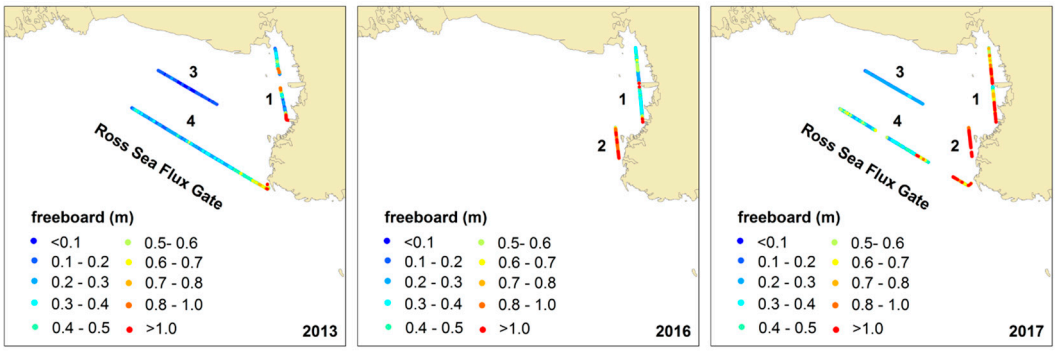

Figure 2. Spatial distribution of total freeboard for each track of OIB (2013, left panel) and IcePod (2016, center panel; 2017, right panel) with the 25 km lowest 2% elevation method.

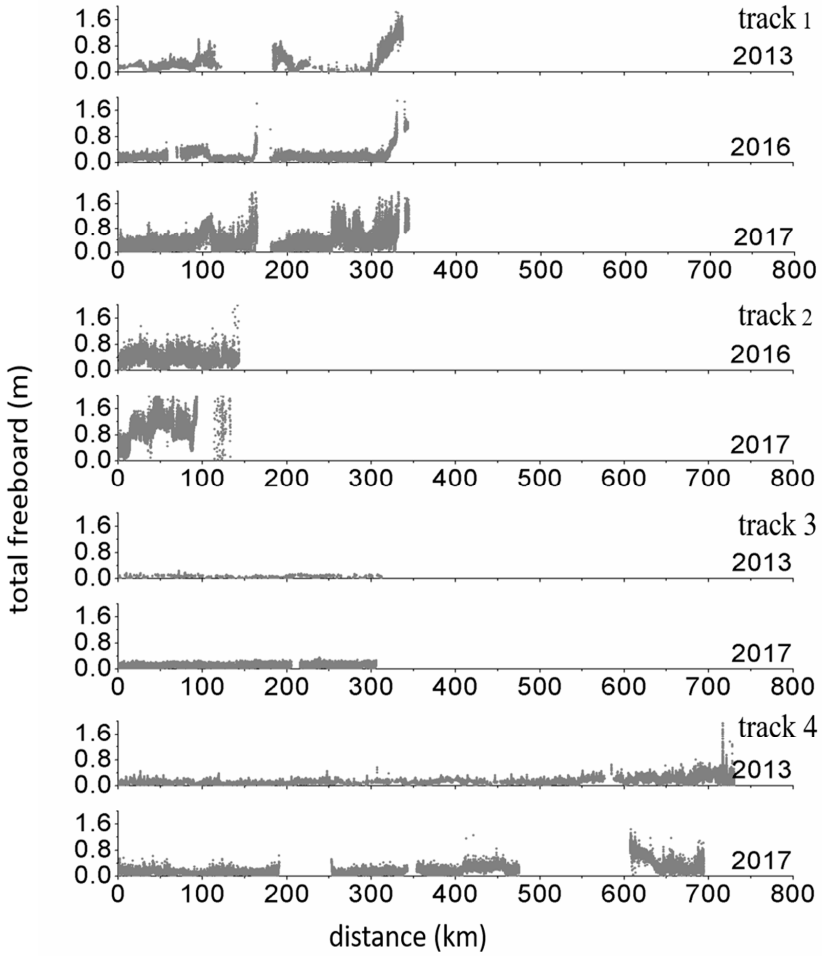

Figure 3. Calculated total freeboard from lidar data along each track of 2013 OIB and 2016–2017 IcePod with the 25 km lowest 2% elevation method. The direction used for distance calculation along each track is indicated by the arrows shown in Figure 1.

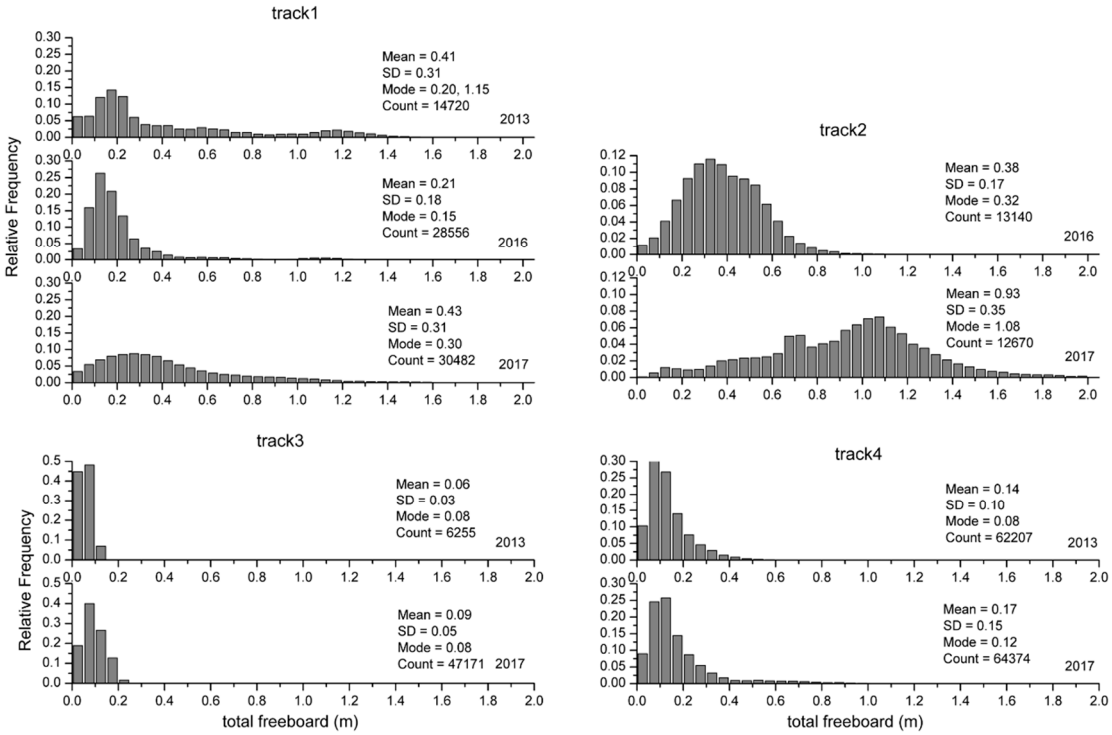

Figure 4. Frequency distributions of total freeboard with mean, SD, mode, and total count number for each track of 2013 OIB and 2016–2017 IcePod data with the 50 km lowest 2% elevation method.

These data allowed us to examine in detail the differences in total freeboard along the tracks across these three years (Figures 3 and 4). In general, the sea ice was thicker in 2017 compared to 2016 and 2013 for all the tracks. For track 1, the first mode for total freeboard was 0.2 m in 2013, 0.15 m in 2016, and 0.3 m in 2017. The first mode usually represents the new and young level ice in the region, and it was the dominant ice type. The mode value of total freeboard of 0.2 m in 2013 was seen with an extended tail to higher thicknesses in the distribution, while in 2016 the mode (0.15 m) had higher frequency and the tail at greater thicknesses was suppressed; in 2017, the mode was 0.3 m but the distribution was wider and flatter, again, an extended tail to higher thicknesses. Over the whole track 1, sea ice in 2017 was overall thicker than in 2016 and 2013, with the thinnest in 2016. The derived mean total freeboard was 0.43 m in 2017, 0.21 m in 2016, and 0.41m in 2013.

For track 2, the sea ice became much thicker in 2017 than in 2016 indicated by higher freeboards with more fluctuations in 2017. The mean total freeboard was 0.38 m with a standard deviation of 0.17 m in 2016 while the mean total freeboard was 0.93 m with a standard deviation of 0.35 m in 2017. The sea ice had two freeboard modes in 2017 (0.70 m, 1.08 m) instead of one in 2016 (0.32 m).

The track 3 shows the thinnest and the least changed sea ice. Sea ice freeboard retained the same mode (0.08 m) in both years but a slightly higher mean in 2017 than in 2013. Very few higher thicknesses were observed, so the distribution was dominated by level ice.

The sea ice along track 4 was, overall, thicker in 2017 than in 2013, i.e., 0.17 versus 0.14 m in mean total freeboard and 0.12 versus 0.08 m in mode for the total freeboard. Greater thicknesses also showed higher frequency in 2017 than in 2016.

Figure 5 and Table 2 show the comparison of total freeboard among three datasets from 2003 to 2017 using the 50 km lowest 2% elevation method. The results indicate that mean freeboard along the near-coastal track 1 was 0.07 m higher in the more recent OIB/IcePod years (2013–2017) than the previous ICESat years (2003–2007). For track 2, mean freeboard was 0.43 m higher in more recent IcePod years (2016–2017) than the previous ICESat years (2004–2008). For track 3, mean freeboard was 0.08 m lower in more recent OIB/IcePod years (2013 and 2017) than the previous ICESat years (2003–2008). For track 4, total freeboard was 0.06 m lower in recent OIB/IcePod years (2013 and 2017)

than the previous ICESat years (2003–2008). The difference of means between the two time periods along each of the four tracks were all statistically significant with greater than 95% confidence based on a bootstrap method [32]. This suggests that, as compared to the ICESat years (2003–2008), sea ice of near-coastal tracks 1 and 2 were thicker, while sea ice of offshore tracks 3 and 4 were thinner in the more recent OIB/IcePod years (2013 and 2017). Whether these changes continue (a trend) or reverse (variability) awaits further analysis of new dataset from the ICESat-2 satellite, launched in late 2018.

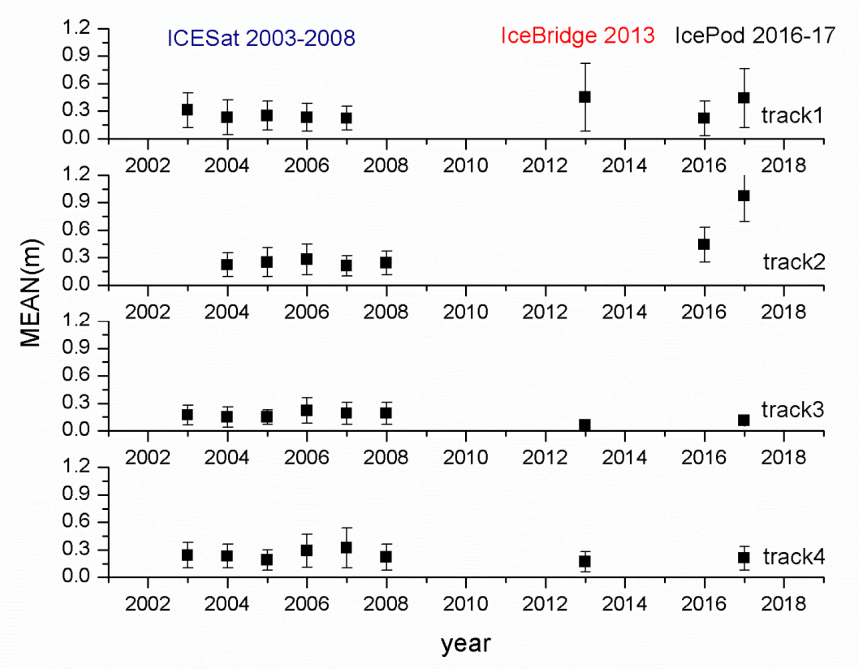

Figure 5. Mean (m) with ±1 standard deviation of total freeboard comparison among the three datasets with the 50 km lowest 2% elevation method.

Table 2. Comparison of mean freeboard between ICESat and more recent OIB/IcePod years with the 50 km lowest 2% elevation method. All differences of means along each track were significant with greater than 95% confidence using a bootstrap method [32].

Tracks	Mean Freeboard (m) (2003–2008)	Mean Freeboard (m) (2013–2017)	Mean Difference (m)
	ICESat (a)	OIB/IcePod (b)	(b − a) ± 1 SD
track 1	0.258 (2003–2007)	0.331 (2013, 2016 and 2017)	0.073 ± 0.003
track 2	0.235 (2004–2008)	0.668 (2016 and 2017)	0.433 ± 0.006
track 3	0.182 (2003–2008)	0.100 (2013 and 2017)	−0.081 ± 0.002
track 4	0.251 (2003–2008)	0.189 (2013 and 2017)	−0.062 ± 0.002

5. Discussion

From the spatial distribution of these four tracks, sea ice along the tracks 1 and 2 were in the coastal regions with characteristics of overall thicker and larger variation in ice types and thickness, while sea ice along track 3 and track 4 were more uniform and overall much thinner in the freer offshore conditions. This indicates that ice deformation and convergence were stronger near the coast. The very thin and level ice of track 3 was the evidence of ice production from the Ross Ice Shelf Polynya (RSP) that was pushed northward. Ice along track 4 was slightly thicker than that along the track 3, since it was further away from the ice production source of the RSP, and it potentially experiences more deformation and convergence during the drifting and transport as shown by the wider distribution and longer tail toward greater thickness. The western portion of the track 4 near the coastal region of Cape

Adare had thicker ice, similar to the ice along the tracks 1 and 2, caused by stronger ice deformation and convergence nearer the coast.

Different sea ice freeboard distributions and modes represent various ice types. The first mode represents the new and young level ice in the region, and it is the dominant ice type. This is mostly produced in the polynyas due to the katabatic winds continuously pushing ice away and new ice forming in the open water behind it. The first mode of freeboard became higher in 2017 when compared to that of 2013 or 2016 for all other tracks except for track 3, where no change was observed. This greater freeboard indicates there was thicker first year ice in 2017.

When comparing the mean freeboard values from more recent OIB/IcePod years to the previous ICESat years in general, we find that sea ice along track 1 and track 2 was thicker in recent OIB/IcePod years than previous ICESat years, while sea ice of track 3 and track 4 was slightly thinner (lower freeboard) in recent OIB/IcePod years than previous years. The Ross Sea ice production and export contribute to the formation of dense shelf water over the continental shelf as the precursor to Antarctic Bottom Water. The Ross Sea fluxgate, separating the shelf from the deep ocean, lies over the 1000 m depth contours. The western end point of the gate is located at Cape Adare, and its eastern end is at Land Bay [33]. The length of the gate is ~1400 km, and the enclosed area is ~490 × 103 km^2 [34]. Martin et al. (2007) [35], Comiso et al. (2011) [36], and Drucker et al. (2011) [37] all found that the polynya ice production approximately equals to the ice export. Calculation of the exported ice volume depends on the ice thickness. As our results show, tracks 1–2 had become thicker, while tracks 3–4 had become slightly thinner in recent years as compared to ICESat years. This may indicate the RSP polynya ice production in November has decreased, usually the last ice production event from RSP of any year [38]. Since track 2 particularly is related to the production of ice in the Terra Nova Bay polynya and its further thickening as it deforms further north, there is high variability in the overall ice production from this source region as the mean total freeboard values are twice (0.93 m) as thicker in 2017 as in 2016 (0.48 m).

Because of the lack of field measurements and the complexity of snow depth in the Ross Sea, it is hard to quantitate the uncertainties. The uncertainties of total freeboard are mainly caused by the different instruments used among ICESat, OIB, and IcePod and the retrieval method used in this study: 2% lowest elevations method to derive local sea level. ICESat's single shot elevation precision over smooth flat surfaces is <3 cm and over ocean elevation has 10.0 ± 1.0 cm bias [39]. The OIB ATM system has 6.6 cm vertical accuracy and 3 cm vertical precision [40]. The IcePod has 25 mm range accuracy. To reduce the discrepancy caused by the three instruments, we resampled the IcePod lidar data into 70 m pixels, which it is comparable to the footprint size of OIB ATM L2 (80 m width by ~60 m along track) and ICESat data resolution (~70 m). In a previous study [22], using high-resolution natural color DMS images (0.1 m at altitude of 457 m) from the 2013 OIB flight, the lidar shots on leads for local sea level were directly identified through the DMS images. Local sea surface height for areas without DMS images were obtained through linear interpolation. This method gave best estimates of local sea surface height and sea ice freeboard. They compared the freeboard values derived from this method to the 2% lowest elevations method to derive local sea surface height and concluded that the 2% lowest elevations method could overestimate the freeboard. They also found that the freeboard value derived from the 2% of the lowest elevations at the 25 km range is better than that at the 50 km range. This is also seen in this study (Figure 6). Previous studies also indicated that the mean freeboard values are less affected than the mode when using different methods [22,41] and all these methods can provide a relatively good spatial distribution although with some differences in absolute values. Therefore, our results using the lowest 2% of 25 km range method probably have provided more accurate mean values than mode values, and our absolute mean values could be slightly higher than reality. Our results still provide very valuable relative values, spatial distribution pattern, and change in pattern of all tracks from the ICESat period (2003–2008), to OIB (2013), and to IcePod (2016–2017), so a fuller picture, although not perfect, helps us in better understanding sea ice changes in recent years. ICESat-2, launched in 2018, is expected to continue this legacy for many years to come.

The resolution of ICESat-2 also allows it to distinguish leads and will allow a better determination of the local sea level reference, similar to the DMS method used for OIB aircraft. A more accurate determination of the freeboard distribution and the resulting ice thickness estimate will emerge [42].

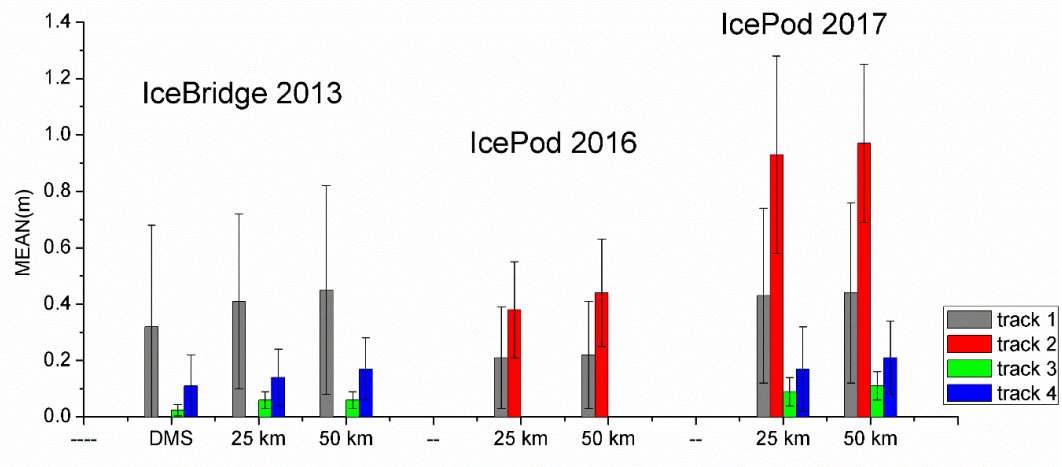

Figure 6. The mean freeboard values with ±1 standard deviation retrieved from different methods. With "DMS", "25 km", and "50 km", respectively, referring to the method combined with ATM and DMS, 25 km and 50 km lowest (2%) elevation methods. All OIB 2013 values are taken from Reference [22].

6. Conclusions

In this study, sea ice total freeboard from IcePod 2016 and 2017 flights over the Ross Sea were derived by using both 25 km and 50 km lowest elevation methods for computing local sea level. The results were further compared with OIB (2013) and ICESat (2003–2008). The pattern of the sea ice spatial distribution supports that new ice produced in coastal polynyas were transported northward by katabatic winds off the ice shelf (sea ice of track 4 is getting thicker than track 3 at the relatively same position of these two parallel tracks in general). Ice of track 1 and track 2 were more fluctuating in these coastal regions while ice of track 3 and track 4 were more uniform in the freer offshore conditions, showing ice deformation was stronger along the coast. Compared to the previous ICESat years, sea ice of near-coastal tracks 1 and 2 were thicker (mean freeboard value was 0.12 m higher for track 1 and 0.47 m higher for track 2), while sea ice of offshore tracks 3 and 4 were slightly thinner in more recent OIB/IcePod years (mean freeboard value was 0.09 m smaller for track 3 and 0.05 m smaller for track 4).

This study shows sea ice was thicker in 2017 compared to 2013 and 2016. But previous studies indicate the decline in yearly average Ross Sea ice extents from 2014 to 2017 [5–7]. Under the background of global warming [43,44], this may seem to represent a contradiction. However, several oceanic, atmospheric, and continental factors can influence sea ice, particularly changes in wind patterns in the Antarctic both on a seasonal basis and, as yet, unknown variability of the katabatic winds that affect ice production in the RSP and TNB and the dynamics of the pack ice. More research around the Ross Sea in the future would help better understand the apparent complex processes between sea ice extent, thickness, and volume within this environment.

Author Contributions: Methodology, L.T.; Resources, K.J.T., R.E.B., C.J.Z. and Y.G.; Supervision, H.X. and S.F.A.; Writing—original draft, L.T.; Writing—review and editing, H.X., S.F.A., K.J.T., R.E.B. and A.M.M.-N. All authors have read and agreed to the published version of the manuscript.

Funding: This research was funded by NASA grant number 80NSSC19M0194 and NSF grant number 134717.

Acknowledgments: We acknowledge a NASA Grant (80NSSC19M0194) to the Center for Advanced Measurements in Extreme Environments at UTSA (H.X, S.F.A, A.M.M.-N., L.T.). We also acknowledge an NSF Grant (134717) to UTSA and LDEO, Polynyas and Ice Production in the Ross Sea for IcePod Flights and Data Analysis (S.F.A., H.X., L.T., Y.G., R.E.B., C.J.Z., K.J.T.).

Conflicts of Interest: The authors declare no conflict of interest.

References

1. Rinke, A.; Maslowski, W.; Dethloff, K.; Clement, J. Influence of sea ice on the atmosphere: A study with an Arctic atmospheric regional climate model. *J. Geophys. Res. Space Phys.* **2006**, *111*, 111. [CrossRef]
2. Dieckmann, G.S.; Hellmer, H.H. The Importance of Sea Ice: An Overview. *Sea Ice* **2010**, *2*, 1–22. [CrossRef]
3. Parkinson, C.; Cavalieri, D. Antarctic sea ice variability and trends, 1979–2010. *The Cryosphere* **2012**, *6*, 871–880. [CrossRef]
4. Parkinson, C.L. A 40-y record reveals gradual Antarctic sea ice increases followed by decreases at rates far exceeding the rates seen in the Arctic. *Proc. Natl. Acad. Sci. USA* **2019**, *116*, 14414–14423. [CrossRef]
5. Turner, J.; Phillips, T.; Marshall, G.J.; Hosking, J.S.; Pope, J.O.; Bracegirdle, T.J.; Deb, P. Unprecedented springtime retreat of Antarctic sea ice in 2016. *Geophys. Res. Lett.* **2017**, *44*, 6868–6875. [CrossRef]
6. Kusahara, K.; Reid, P.; Williams, G.D.; Massom, R.A.; Hasumi, H. An ocean-sea ice model study of the unprecedented Antarctic sea ice minimum in 2016. *Environ. Res. Lett.* **2018**, *13*, 084020. [CrossRef]
7. Stuecker, M.F.; Bitz, C.M.; Armour, K.C. Conditions leading to the unprecedented low Antarctic sea ice extent during the 2016 austral spring season. *Geophys. Res. Lett.* **2017**, *44*, 9008–9019. [CrossRef]
8. Gordon, A.L.; Comiso, J.C. Polynyas in the Southern Ocean. *Sci. Am.* **1988**, *258*, 90–97. [CrossRef]
9. Maksym, T.; Stammerjohn, S.; Ackley, S.; Massom, R.A. Antarctic Sea Ice—A Polar Opposite? *Oceanography* **2012**, *25*, 140–151. [CrossRef]
10. Lange, M.A.; Eicken, H. The sea ice thickness distribution in the northwestern Weddell Sea. *J. Geophys. Res. Space Phys.* **1991**, *96*, 4821. [CrossRef]
11. Haas, C.; Gerland, S.; Eicken, H.; Miller, H. Comparison of sea-ice thickness measurements under summer and winter conditions in the Arctic using a small electromagnetic induction device. *Geophysics* **1997**, *62*, 749–757. [CrossRef]
12. Yi, D.; Zwally, H.J.; Robbins, J.W. ICESat observations of seasonal and interannual variations of sea-ice freeboard and estimated thickness in the Weddell Sea, Antarctica (2003–2009). *Ann. Glaciol.* **2011**, *52*, 43–51. [CrossRef]
13. Laxon, S.W.; Giles, K.A.; Ridout, A.L.; Wingham, D.J.; Willatt, R.; Cullen, R.; Kwok, R.; Schweiger, A.; Zhang, J.; Haas, C.; et al. CryoSat-2 estimates of Arctic sea ice thickness and volume. *Geophys. Res. Lett.* **2013**, *40*, 732–737. [CrossRef]
14. Xie, H.; Tekeli, A.E.; Ackley, S.F.; Yi, D.; Zwally, H.J. Sea ice thickness estimations from ICESat Altimetry over the Bellingshausen and Amundsen Seas, 2003-2009. *J. Geophys. Res. Oceans* **2013**, *118*, 2438–2453. [CrossRef]
15. Li, H.; Xie, H.; Kern, S.; Wan, W.; Ozsoy, B.; Ackley, S.; Hong, Y. Spatio-temporal variability of Antarctic sea-ice thickness and volume obtained from ICESat data using an innovative algorithm. *Remote Sens. Environ.* **2018**, *219*, 44–61. [CrossRef]
16. Kwok, R.; Cunningham, G.F.; Manizade, S.; Krabill, W. Arctic sea ice freeboard from IceBridge acquisitions in 2009: Estimates and comparisons with ICESat. *J. Geophys. Res. Space Phys.* **2012**, *117*, 117. [CrossRef]
17. Kwok, R.; Cunningham, G.F.; Zwally, H.J.; Yi, D. Ice, Cloud, and land Elevation Satellite (ICESat) over Arctic sea ice: Retrieval of freeboard. *J. Geophys. Res. Space Phys.* **2007**, *112*, 112. [CrossRef]
18. Xie, H.; Ackley, S.; Yi, D.; Zwally, H.; Wagner, P.; Weissling, B.; Lewis, M.; Ye, K. Sea-ice thickness distribution of the Bellingshausen Sea from surface measurements and ICESat altimetry. *Deep. Sea Res. Part II Top. Stud. Oceanogr.* **2011**, *58*, 1039–1051. [CrossRef]
19. Studinger, M. *IceBridge ATM L2 Icessn Elevation, Slope, and Roughness, Version 2*; NASA Distrib. Active Archive Center, Nat. Snow Ice Data Center: Boulder, CO, USA, 2016.
20. Ackley, S.F.; Stammerjohn, S.; Maksym, T.; Smith, M.; Cassano, J.; Guest, P.; Tison, J.-L.; Delille, B.; Loose, B.; Sedwick, P.; et al. Sea-ice production and air/ice/ocean/biogeochemistry interactions in the Ross Sea during the PIPERS 2017 autumn field campaign. *Ann. Glaciol.* **2020**, 1–15. [CrossRef]
21. Bell, R.; Frearson, N.; Zappa, C.; Tinto, K.; Das, I.; Dhakal, T.; Bertinato, C.; Dong, L.; Brown, S.; Le Bel, D. IcePod: Imaging Ice-Ocean Process from Top to Bottom. In Proceedings of the AGU Fall Meeting Abstracts, San Francisco, CA, USA, 15 December 2014.
22. Tian, L.; Xie, H.; Ackley, S.F.; Tang, J.; Mestas-Nuñez, A.M.; Wang, X. Sea-ice freeboard and thickness in the Ross Sea from airborne (IceBridge 2013) and satellite (ICESat 2003–2008) observations. *Ann. Glaciol.* **2020**, 1–16. [CrossRef]
23. Dinniman, M.S.; Klinck, J.M.; Smith, W.O., Jr. Cross-shelf exchange in a model of the Ross Sea circulation and biogeochemistry. *Deep. Sea Res. Part II Top. Stud. Oceanogr.* **2003**, *50*, 3103–3120. [CrossRef]

24. Boghosian, A.L.; Pratt, M.J.; Becker, M.K.; Cordero, S.I.; Dhakal, T.; Kingslake, J.; Locke, C.D.; Tinto, K.J.; Bell, R.E. Inside the ice shelf: Using augmented reality to visualise 3D lidar and radar data of Antarctica. *Photogramm. Rec.* **2019**, *34*, 346–364. [CrossRef]
25. Krabill, W. *IceBridge ATM L1B Elevation and Return Strength, Version 2*; NASA DAAC at the National Snow and Ice Data Center: Boulder, CO, USA, 2013.
26. Zwally, H.; Schütz, B.; Abdalati, W.; Abshire, J.; Bentley, C.; Brenner, A.; Bufton, J.; Dezio, J.; Hancock, D.; Harding, D.; et al. ICESat's laser measurements of polar ice, atmosphere, ocean, and land. *J. Geodyn.* **2002**, *34*, 405–445. [CrossRef]
27. Kwok, R.; Zwally, H.J.; Yi, D. ICESat observations of Arctic sea ice: A first look. *Geophys. Res. Lett.* **2004**, *31*, 31. [CrossRef]
28. Kern, S.; Spreen, G. Uncertainties in Antarctic sea-ice thickness retrieval from ICESat. *Ann. Glaciol.* **2015**, *56*, 107–119. [CrossRef]
29. Stewart, R.H. *Introduction to Physical Oceanography*; Dep. of Oceanogr., Tex. A&M Univ.: College Station, TX, USA, 2008.
30. Andersen, O.; Knudsen, P.; Stenseng, L. The DTU13 MSS (Mean Sea Surface) and MDT (Mean Dynamic Topography) from 20 years of satellite altimetry. In Proceeding of the International Association of Geodesy Symposia, Heidelberg, Germany, 13 August 2015.
31. Zwally, H.J.; Yi, D.; Kwok, R.; Zhao, Y.; Kwok, R. ICESat measurements of sea ice freeboard and estimates of sea ice thickness in the Weddell Sea. *J. Geophys. Res. Space Phys.* **2008**, *113*, 113. [CrossRef]
32. Nayak, M.R.; Emery, W.J.; Thomson, R.E.; Voulgaris, G. Data Analysis Methods in Physical Oceanography. *Estuaries* **1999**, *22*, 728–730. [CrossRef]
33. Kwok, R.; Pang, S.S.; Kacimi, S.; Kwok, R. Sea ice drift in the Southern Ocean: Regional patterns, variability, and trends. *Elem. Sci. Anth.* **2017**, *5*, 32. [CrossRef]
34. Kwok, R. Ross Sea Ice Motion, Area Flux, and Deformation. *J. Clim.* **2005**, *18*, 3759–3776. [CrossRef]
35. Martin, S.; Drucker, R.S.; Kwok, R. The areas and ice production of the western and central Ross Sea polynyas, 1992–2002, and their relation to the B-15 and C-19 iceberg events of 2000 and 2002. *J. Mar. Syst.* **2007**, *68*, 201–214. [CrossRef]
36. Comiso, J.C.; Kwok, R.; Martin, S.; Gordon, A.L. Variability and trends in sea ice extent and ice production in the Ross Sea. *J. Geophys. Res. Space Phys.* **2011**, *116*, 116. [CrossRef]
37. Drucker, R.; Martin, S.; Kwok, R. Sea ice production and export from coastal polynyas in the Weddell and Ross Seas. *Geophys. Res. Lett.* **2011**, *38*, 38. [CrossRef]
38. Dai, L.; Xie, H.; Ackley, S.F.; Mestas-Nuñez, A.M. Ice Production in Ross Ice Shelf Polynyas during 2017–2018 from Sentinel–1 SAR Images. *Remote Sens.* **2020**, *12*, 1484. [CrossRef]
39. Urban, T.; Schutz, B.E. ICESat sea level comparisons. *Geophys. Res. Lett.* **2005**, *32*, 32. [CrossRef]
40. Martin, C.F.; Krabill, W.B.; Manizade, S.S.; Russell, R.L.; Sonntag, J.G.; Swift, R.N.; Yungel, J.K. *Airborne Topographic Mapper Calibration Procedures and Accuracy Assessment*; NASA Tech. Memo. TM–2012-21; National Aeronautics and Space Administration, Goddard Space Flight Center: Greenbelt, MD, USA, 2012.
41. Geiger, C.A.; Mueller, H.-R.; Samluk, J.P.; Bernstein, E.R.; Richter-Menge, J. Impact of spatial aliasing on sea-ice thickness measurements. *Ann. Glaciol.* **2015**, *56*, 353–362. [CrossRef]
42. Kwok, R.; Kacimi, S.; Markus, T.; Kurtz, N.T.; Studinger, M.; Sonntag, J.G.; Manizade, S.S.; Boisvert, L.N.; Harbeck, J.P. ICESat-2 Surface Height and Sea Ice Freeboard Assessed With ATM Lidar Acquisitions From Operation IceBridge. *Geophys. Res. Lett.* **2019**, *46*, 11228–11236. [CrossRef]
43. Pachauri, R.K.; Reisinger, A. *IPCC Fourth Assessment Report*; IPCC: Geneva, Switzerland, 2007.
44. Shakun, J.D.; Clark, P.U.; He, F.; Marcott, S.A.; Mix, A.C.; Liu, Z.; Otto-Bliesner, B.; Schmittner, A.; Bard, E. Global warming preceded by increasing carbon dioxide concentrations during the last deglaciation. *Nature* **2012**, *484*, 49–54. [CrossRef] [PubMed]